

Regions of Applicability of Approximate Formulations of Neutrino Oscillations in Matter

Mikkel B. Johnson

Los Alamos National Laboratory, Los Alamos, NM 87545

Ernest M. Henley

Department of Physics, University of Washington, Seattle, WA 98195

Leonard S. Kisslinger

Department of Physics, Carnegie-Mellon University, Pittsburgh, PA 15213

We examine the reliability of the theoretical methods presently used for analysis and prediction of neutrino oscillation phenomena. Of particular interest are the limitations imposed by branch points when expansions in one of the small parameters of the Standard Neutrino Model (SNM) are made to obtain tractable results. Our evaluation compares the approximate oscillation probabilities for flavor-changing transitions in the (ν_e, ν_μ) sector to exact results obtained from a recently-developed exact analytical representation of neutrino oscillations in matter within the SNM. From our numerical comparisons, we are able to identify regions where the existing approaches can be improved to take full advantage of the higher quality data expected at future neutrino facilities.

PACS Indices: 11.3.Er, 14.60.Lm, 13.15.+g

Keywords:

I. INTRODUCTION

In this paper, we explore the theoretical errors of simple expressions for oscillation probabilities found from approximate formulations for the purpose of analysis and prediction of experiment at current and proposed future neutrino facilities. Our assessment includes the interaction of neutrinos with electrons shown to be essential by Wolfenstein in 1978 [1] and later identified by Mikheyev and Smirnov [2] as a likely explanation of the deficit of solar neutrinos discovered experimentally by Davis [3, 4]. Subsequent to the work of Wolfenstein, the effect of matter on neutrino oscillations has been commonly explored using exact computer simulations. Computer simulations of neutrino oscillations in matter are found in Refs. [5] and references therein. Such numerical studies are preferred when density profiles with a spatial dependence are essential.

Our assessment of expressions for the oscillation probability in the flavor-changing (ν_e, ν_μ) sector is made by comparing the approximate expressions to corresponding exact analytical expressions for the oscillation probability of 3 coupled Dirac neutrinos. The expressions assessed include not only neutrino oscillation probabilities found in Refs. [6–8] but also neutrino oscillation probabilities from yet another approximate formulation we propose based on expressions for the oscillation probability found in

our recently published paper [9] evaluated with ξ -expanded eigenvalues.

The exact analytical expressions for the oscillation probability used for the comparison are obtained from our recently-developed Hamiltonian formulation [9]. They are algebraic functions of the parameters of the Standard Neutrino Model [10] (SNM), the neutrino eigenvalues, and include matter effects. The expressions were obtained by using the Lagrange interpolation formula [11] to exponentiate the neutrino Hamiltonian and have been used to verify our own exploratory studies [12–15] that used the expressions appearing in Refs. [6–8].

In Sect. V, we review the simple analytical results presently available [6–8], and in Sect. VI, we discuss the assessment itself. Then, in Sect. VII, we assess the oscillation probabilities found in Refs. [6–8]. This assessment, which appears in Sect. VIII, confirms the finding of Ref. [9] that the accuracy of the approximate analytic results of Refs. [6–8] is limited by the presence of branch points in the analytic structure of the eigenvalues of neutrinos propagating in matter.

The analysis in Sect. VIII also suggests that the simple expressions for neutrino oscillation probability we find using our Hamiltonian formulation [9] are accurate to a few percent in all regions. It also identifies regions where the approximate analytical results are reliable by making numerical comparisons to exact results [9]. The approximate expressions we propose are conservatively estimated there to be accurate to a few percent within essentially all regions of interest. Approximate expressions of such accuracy would, of course, obviate the need for exact

computer simulations under many circumstances.

Combining the results of Sect. VII with numerical results presented in Ref. [9], we identify the regions where the approximate oscillation probabilities found from our proposed formulation are more accurate than those of Refs. [6–8]. In a future publication [16], we show how to construct such approximate oscillation probabilities in practice guided by the assessment made here.

II. NEUTRINO DYNAMICS

The dynamics of the three known neutrinos and their corresponding anti-neutrinos in matter is determined by the time-dependent Schroedinger equation,

$$i \frac{d}{dt} |\nu(t)\rangle = H_\nu |\nu(t)\rangle, \quad (1)$$

where the neutrino Hamiltonian H_ν ,

$$H_\nu = H_{0\nu} + H_1, \quad (2)$$

consists of a piece $H_{0\nu}$ describing neutrinos in the vacuum and a piece H_1 describing their interaction with matter.

The solutions of Eq. (1) may be expressed in terms of stationary-state solutions of the eigenvalue (EV) equation

$$H_\nu |\nu_{mi}\rangle = E_i |\nu_{mi}\rangle, \quad (3)$$

where the label “ m ” indicates neutrino mass eigenstates, as distinguished from their flavor states sometimes denoted the label “ f ”. Neutrinos are produced and detected in states of good flavor.

In operator form, the dynamics of neutrinos may be expressed in terms of the time-evolution operator $S(t', t)$, which describes completely the evolution of states from time t to t' and also satisfies the time-dependent Schroedinger equation.

We will examine neutrinos propagating in a uniform medium for interactions constant not only in space but also time. Because the Hamiltonian is then translationally invariant, attention may be restricted to states, both in the vacuum and in matter, characterized by momentum \vec{p} and therefore having the overall r -dependence $e^{i\vec{p}\cdot\vec{r}}$. In this case, expressions may be simplified by suppressing the overall plane wave, a convention we adopt.

For time-independent interactions, $S(t', t)$,

$$S(t', t) = e^{-iH_\nu(t'-t)}, \quad (4)$$

depends on time only through the time *difference* $t' - t$. Then, written in terms of the stationary state solutions $|\nu_{mi}\rangle$ of Eq. (1),

$$S(t', t) = \sum_i |\nu_{mi}\rangle e^{-iE_i(t'-t)} \langle \nu_{mi}|. \quad (5)$$

We assume here that that neutrinos and anti-neutrinos represented by $|\nu_{mi}^0\rangle$ and $|\bar{\nu}_{mi}^0\rangle$, respectively, are the structureless elementary Dirac fields of the the Standard Neutrino Model [10]. For this reason the theory is invariant under CPT, so the mass of an anti-neutrino in the vacuum is the same as that for its corresponding neutrino.

The case of main interest for many situations is the ultra-relativistic limit, $|\vec{p}| \gg m^2$ (we take the speed of light $c = 1$). For ultra-relativistic neutrinos in the laboratory frame, the energy of a neutrino in the vacuum becomes

$$E_i^0 \approx |\vec{p}| + \frac{m_i^2}{2E}, \quad (6)$$

where m_i is its mass the vacuum. Similarly, E_i appearing in Eq. (3) may be written

$$E_i \approx |\vec{p}| + \frac{M_i^2}{2E}, \quad (7)$$

where M_i is its mass in the medium. Thus, in this limit and in dimensionless variables,

$$\hat{E}_i \rightarrow \frac{M_i^2 - m_1^2}{m_3^2 - m_1^2} \quad (8)$$

and

$$\hat{H}_{0\nu} \rightarrow \begin{pmatrix} 0 & 0 & 0 \\ 0 & \alpha & 0 \\ 0 & 0 & 1 \end{pmatrix} \quad (9)$$

with

$$\alpha \equiv \frac{m_2^2 - m_1^2}{m_3^2 - m_1^2}. \quad (10)$$

In this limit, the distance L from the source to the detector corresponding to $S(t', t)$ in Eq. (4) is

$$L = t' - t. \quad (11)$$

The time-evolution operator, Eq. (4), expressed in dimensionless variables is then,

$$S(L) = e^{-iH_\nu(t'-t)} = e^{2i\hat{E}_1\Delta L} e^{-2i\hat{H}_\nu\Delta L}, \quad (12)$$

where \hat{H}_ν is the full neutrino Hamiltonian expressed in dimensionless variables, and where

$$\Delta_L \equiv \frac{L(m_3^2 - m_1^2)}{4E} . \quad (13)$$

III. THE NEUTRINO INTERACTION AND THE STANDARD NEUTRINO MODEL

Flavor and mass states are related by the neutrino analog of the familiar CKM unitary matrix U ,

$$\nu_f = U \nu_m . \quad (14)$$

The matrix U is often parametrized in terms of three mixing angles $(\theta_{12}, \theta_{13}, \theta_{23})$ and a phase δ_{cp} characterizing CP violation, taking the form,

$$U \equiv \begin{pmatrix} c_{12}c_{13} & s_{12}c_{13} & s_{13}e^{-i\delta_{cp}} \\ U_{21} & U_{22} & s_{23}c_{13} \\ U_{31} & U_{32} & c_{23}c_{13} \end{pmatrix} , \quad (15)$$

where,

$$\begin{aligned} U_{21} &= -s_{12}c_{23} - c_{12}s_{23}s_{13}e^{i\delta_{cp}} \\ U_{22} &= c_{12}c_{23} - s_{12}s_{23}s_{13}e^{i\delta_{cp}} \\ U_{31} &= s_{12}s_{23} - c_{12}c_{23}s_{13}e^{i\delta_{cp}} \\ U_{32} &= -c_{12}s_{23} - s_{12}c_{23}s_{13}e^{i\delta_{cp}} , \end{aligned} \quad (16)$$

and where the index $i = 1$ in U_{ij} corresponds to the electron (e) neutrino, $i = 2$ to the muon (μ) neutrino, and $i = 3$ to the tau (τ) neutrino. The standard abbreviations, $s_{12} \equiv \sin \theta_{12}$, $c_{12} \equiv \cos \theta_{12}$, *etc* have been used.

The perturbing Hamiltonian H_1 is determined by the interaction between electron neutrino flavor states and the electrons of the medium. Expressed as matrix,

$$H_1 = U^{-1} \begin{pmatrix} V & 0 & 0 \\ 0 & 0 & 0 \\ 0 & 0 & 0 \end{pmatrix} U , \quad (17)$$

with $V = \pm\sqrt{2}G_F n_e$ and n_e the electron number density in matter.

For electrically neutral matter consisting of protons, neutrons, and electrons, the electron density n_e is the same as the proton density n_p ,

$$\begin{aligned} n_e &= n_p \\ &= RA , \end{aligned} \quad (18)$$

where $A = N + Z$ is the average total nucleon number density and $R = Z/A$ is the average proton-

nucleon ratio. In the earth's mantle, the dominant constituents of matter are the light elements so $R \approx 1/2$; in the surface of a neutron star $R \ll 1$. Matrix elements of H_1 are thus

$$\langle M(k) | H_1 | M(k') \rangle = U_{1k}^* V U_{1k'} . \quad (19)$$

Using the well-known expression for V , we find the corresponding the (dimensionless) interaction strength \hat{A} of neutrinos and anti-neutrinos with matter to be,

$$\hat{A} = \pm 6.50 \cdot 10^{-2} R E [\text{GeV}] \rho [\text{gm/cm}^3] , \quad (20)$$

with $E[\text{GeV}]$ being the neutrino beam energy E (in GeV) and $\rho[\text{gm/cm}^3]$ the average total density (in gm/cm^3) of matter through which the neutrino beam passes on its way to the detector. For our experiments close to the earth's surface, the appropriate density is mean density of the earth's mantle,

$$\begin{aligned} \rho [\text{gm/cm}^3] &= \rho_0 \\ &\approx 3 . \end{aligned} \quad (21)$$

We adopt the SNM [10], given next, to complete our description of the neutrino Hamiltonian. Most of the parameters of the SNM are consistent with global fits to neutrino oscillation data with relatively good precision [12, 13]. These include the neutrino mass differences,

$$\begin{aligned} m_2^2 - m_1^2 &\equiv \delta m_{21}^2 \\ &= 7.6 \times 10^{-5} \text{ eV}^2 \end{aligned} \quad (22)$$

and

$$\begin{aligned} m_3^2 - m_1^2 &\equiv \delta m_{31}^2 \\ &= 2.4 \times 10^{-3} \text{ eV}^2 , \end{aligned} \quad (23)$$

which corresponds to

$$\begin{aligned} \alpha &\equiv \frac{\delta m_{21}^2}{\delta m_{31}^2} \\ &= 3.17 \times 10^{-2} . \end{aligned} \quad (24)$$

The mixing angles θ are also determined from experiment. In the SNM, the value of θ_{23} ,

$$\theta_{23} = \pi/4 , \quad (25)$$

is the best-fit value from Ref. [17], and θ_{12} ,

$$\theta_{12} = \pi/5.4 , \quad (26)$$

is consistent with the recent analysis of Ref. [18]. The mixing angle θ_{13} is known to be small ($\theta_{13} <$

0.18 at the 95% confidence level) but until recently its precise value is uncertain. Results from the Daya Bay project [19] have measured its value quite accurately, $\sin \theta_{13} \approx 0.15$, which we adopt to determine our value for θ_{13} ,

$$\theta_{13} = 0.151 . \quad (27)$$

This fixes $R_p \equiv \sin^2 \theta_{13} / \alpha \approx 0.711$. The CP violating phase is not known at all and will one of the major interests at future neutrino facilities.

Using the value of δm_{21}^2 from the SNM, Δ_L , defined in Eq. (13) becomes, in the high-energy limit,

$$\Delta_L \approx 3.05 \times 10^{-3} \frac{L[\text{Km}]}{E[\text{GeV}]} . \quad (28)$$

Here $L[\text{Km}]$ is the baseline and $E[\text{GeV}]$ is the neutrino beam energy

IV. EXACT ANALYTIC EXPRESSIONS FOR $\mathcal{P}(\nu_i \rightarrow \nu_f)$

Our Hamiltonian formulation of neutrino oscillations [9] leads to exact, closed-form, analytical expressions neutrino oscillation probability expressed as the sum of four partial oscillation probabilities,

$$\begin{aligned} \mathcal{P}(\nu_a \rightarrow \nu_b) = & \delta(a, b) + P_{\sin \delta}^{ab} + P_0^{ab} + P_{\cos \delta}^{ab} \\ & + P_{\cos^2 \delta}^{ab} , \end{aligned} \quad (29)$$

representing the dependence of the oscillation probability on the CP violating phase δ_{cp} . The partial oscillation probabilities are given in Appendix A, where they are expressed as explicit functions of the neutrino medium modified neutrino eigenvalues $\hat{\hat{E}}_\ell$ and a set of coefficients $w_{i;\ell}^{ab}$.

Equations determining the exact eigenvalues, and various approximations to them, appear in Appendix A 1. Finally, in Appendix B, explicit algebraic expressions for the coefficients $w_{i;\ell}^{ab}$ for all transitions $\nu_a \leftrightarrow \nu_b$ are given in terms of the parameters of the SNM.

V. PERTURBATIVE EXPANSIONS OF $\mathcal{P}(\nu_i \rightarrow \nu_f)$

The fact that α and $\sin \theta_{13}$ are naturally small in the SNM commonly motivates approximation schemes [6–8, 20] based on first-order Taylor se-

ries expansions in one of these small parameters, ξ'_i (where ξ'_i stands for α or $\sin^2 \theta_{13}$). For example, in Refs. [7, 8] the oscillation probability is expanded in $\sin^2 \theta_{13}$. Reference [6] makes use of an expansion in the small parameter α . In both publications, the only transitions considered are those in the (e, μ) sector.

Although the expansions have the advantage of simplifying the theory, their use comes at a price: neither expansion gives an accurate representations for all regions of the interaction strength \hat{A} , including some regions of critical importance. The origin of this inaccuracy is the presence of branch points in the neutrino eigenvalues [9]. We refer to these truncated ξ_i -expanded oscillation probabilities of Refs. [6–8] as “full” results. In addition to his full result, Freund also introduces an *ad hoc* “patched” result to repair spuriousity of different origin.

In this section, we review the results for the oscillation probability in the (e, μ) sector obtained in Refs. [6–8, 20]. In later sections, we then compare their oscillation probabilities numerically to the corresponding exact expressions obtained from our Hamiltonian formulation evaluated with both the exact neutrino eigenvalues and with the ξ_i -expanded eigenvalues.

A. Full Result of Freund

In his work, Freund gives [6] two versions of the oscillation probabilities based on this α -expansion, a full version and a patched version. As in our own work, the oscillation probabilities are expressed as a functional of the flavor mixing angles and the CP-violating phase that define the neutrino CKM mixing matrix, the neutrino mass differences squared, and the strength of the neutrino interaction with matter. Consequently, Freund makes simplifications [6] in two stages. The first stage is to expand the eigenvalues, and the second stage is to use these results in an expansion of the oscillation probability.

Freund’s α -expanded eigenvalues, given in Eqs. (18,19) of Ref. [6] are identical to those of Eq. (??) in the Appendix. Numerical comparison to the exact result confirms that $\hat{\hat{E}}_1^\alpha$ and $\hat{\hat{E}}_2^\alpha$ are poor representations of the corresponding exact results in the vicinity of the branch point at $\hat{A} = 0$.

Freund’s full α -expanded partial oscillation probabilities in the $\nu_e \rightarrow \nu_\mu$ sector are,

$$\begin{aligned}
P_0^{e\mu}(\Delta_L, \hat{A}) &= \sin^2 \theta_{23} \frac{\sin^2 2\theta_{13}}{\hat{C}_\alpha^2} \sin^2 \Delta_L \hat{C}_\alpha \\
P_1^{e\mu}(\Delta_L, \hat{A}) &= -\alpha \frac{1 - \hat{A} \cos 2\theta_{13}}{\hat{C}_\alpha^3} \sin^2 \theta_{12} \sin^2 2\theta_{13} \sin^2 \theta_{23} \Delta_L \\
&\quad \times \sin 2\hat{C}_\alpha \Delta_L + \alpha \frac{2\hat{A}(-\hat{A} + \cos 2\theta_{13})}{\hat{C}_\alpha^4} \sin^2 \theta_{12} \sin^2 2\theta_{13} \sin^2 \theta_{23} \sin^2 \Delta_L \hat{C}_\alpha \\
P_{\sin \delta}^{e\mu}(\Delta_L, \hat{A}) &= \frac{\alpha}{2} \sin \delta_{cp} \frac{\cos \theta_{13} \sin 2\theta_{12} \sin 2\theta_{13} \sin 2\theta_{23}}{\hat{A} \hat{C}_\alpha \cos^2 \theta_{13}} \sin \hat{C}_\alpha \Delta_L \\
&\quad \times [\cos \hat{C}_\alpha \Delta_L - \cos(1 + \hat{A}) \Delta_L] \\
P_{\cos \delta}^{e\mu}(\Delta_L, \hat{A}) &= \frac{\alpha}{2} \cos \delta_{cp} \frac{\cos \theta_{13} \sin 2\theta_{12} \sin 2\theta_{13} \sin 2\theta_{23}}{\hat{A} \hat{C}_\alpha \cos^2 \theta_{13}} \sin \Delta_L \hat{C}_\alpha \\
&\quad \times [\sin(1 + \hat{A}) \Delta_L \mp \sin \hat{C}_\alpha \Delta_L] \\
P_2^{e\mu}(\Delta_L, \hat{A}) &= \alpha \frac{\mp 1 + \hat{C}_\alpha \pm \hat{A} \cos 2\theta_{13}}{2\hat{C}_\alpha^2 \hat{A} \cos^2 \theta_{13}} \cos \theta_{13} \sin 2\theta_{12} \sin 2\theta_{13} \\
&\quad \times \sin 2\theta_{23} \sin^2 \hat{C}_\alpha \Delta_L \\
P_3^{e\mu}(\Delta_L, \hat{A}) &= \alpha^2 \frac{2\hat{C}_\alpha \cos^2 \theta_{23} \sin^2 2\theta_{12}}{\hat{A}^2 \cos^2 \theta_{13} (\mp \hat{A} + \hat{C}_\alpha \pm \cos 2\theta_{13})} \sin^2 \frac{1}{2} (1 + \hat{A} \mp \hat{C}_\alpha) \Delta_L .
\end{aligned} \tag{30}$$

The lower sign applies above the atmospheric resonance, and the upper sign applies below it. The term P_3 , of order α^2 , is a correction term that improves the overall accuracy. To obtain these results, Freund linearized the oscillating terms over α , the solar mass-squared difference. His results thus apply only for baselines where

$$\alpha \Delta_L < 1 . \tag{31}$$

In addition to observing that his expressions for the α -expanded eigenvalues are not valid for $|\hat{A}| < \alpha$, Freund [6] notes a shortcoming of the technique he uses when there are resonances. The advantage of this technique is the possibility of extracting the mixing angles, as modified by the medium, from the unitary transformation that diagonalizes the Hamiltonian.

However, in order to construct this transformation, it is necessary to keep track of the ordering of the *eigenvectors* across resonances that characterize the transition of interest. In the presence of resonances, the eigenvectors must be exchanged at their position to preserve the proper ordering. Unavoidably, doing so introduces discontinuities. This is the source of the flip of sign at the location of the

atmospheric resonance, $\hat{A} = \cos 2\theta_{13}$, in Eq. (30). This discontinuity is the price one pays to use this method. We note in passing that these discontinuities are avoided in our Hamiltonian approach [9] by using the Lagrange interpolation formula.

Freund examines the accuracy of the result given in Eq. (30) by comparing to exact numerical simulations for a specific baseline and range of energies encompassing the atmospheric resonance. From these results, given in his Fig. 1, he concludes that the loss of precision of his full α -expanded is less serious for small values of θ_{13} , such as the value $\theta_{13} \approx 0.1$, which is the CHOOZ bound. Unfortunately, the recent result Daya Bay [19] gives a larger result, $\sin \theta_{13} \approx 0.15$, which makes the use of Freund's full result somewhat awkward.

B. Patched Result of Freund

Freund identifies the source of the inaccuracies to be the sub-leading terms in θ_{13} within his representation. Based on his understanding, Freund proposes a “patched” result that he argues would be more appropriate than his full result when it fails. This leads to his “patched” expressions,

$$\begin{aligned}
P_0^{e\mu}(\Delta_L, \hat{A}) &= \sin^2 \theta_{23} \frac{\sin^2 2\theta_{13}}{(\hat{A} - 1)^2} \sin^2 (\hat{A} - 1) \Delta_L \\
P_{\sin \delta}^{e\mu}(\Delta_L, \hat{A}) &= \alpha \sin \delta_{cp} \frac{\cos \theta_{13} \sin 2\theta_{12} \sin 2\theta_{13} \sin 2\theta_{23}}{\hat{A}(\hat{A} - 1)} \sin \Delta_L \sin \hat{A} \Delta_L \sin (\hat{A} - 1) \Delta_L \\
P_{\cos \delta}^{e\mu}(\Delta_L, \hat{A}) &= \alpha \cos \delta_{cp} \frac{\cos \theta_{13} \sin 2\theta_{12} \sin 2\theta_{13} \sin 2\theta_{23}}{\hat{A}(\hat{A} - 1)} \cos \Delta_L \sin \hat{A} \Delta_L \sin (\hat{A} - 1) \Delta_L \\
P_3^{e\mu}(\Delta_L, \hat{A}) &= \alpha^2 \frac{\cos^2 \theta_{23} \sin^2 2\theta_{12}}{\hat{A}^2} \sin^2 \hat{A} \Delta_L ,
\end{aligned} \tag{32}$$

which appear in Eq. (38a-38d) of Ref. [6]. Freund notes that the θ_{13} dependence is improved by retaining $P_3^{e\mu}(\Delta_L, \hat{A})$. He neglects $P_1^{e\mu}(\Delta_L, \hat{A})$ and $P_2^{e\mu}(\Delta_L, \hat{A})$ because he finds them much smaller than $P_{\sin \delta}^{e\mu}(\Delta_L, \hat{A})$ and $P_{\cos \delta}^{e\mu}(\Delta_L, \hat{A})$.

C. Full Result of AHLO

The AHLO neutrino oscillation probability,

$$\begin{aligned}
\mathcal{P}(\nu_a \rightarrow \nu_b) &\equiv P^{\nu_a \rightarrow \nu_b} \\
&= |S^{ab}|^2 ,
\end{aligned} \tag{33}$$

is determined from an expansion of time-evolution operator S^{ab} in $\sin^2 \theta_{13}$. The approach was originally proposed in Refs [7, 8], and details of its implementation are given in Appendix A of In Ref. [7]. Their final result is a first-order perturbation theory expansion of S^{ab} in $\sin^2 \theta_{13}$, denoted there $S'(t, t_0)$ and is equivalent to a first-order Taylor expansion of the *entire* $\mathcal{P}(\nu_i \rightarrow \nu_f)$ about $\xi_i = \sin^2 \theta_{13} = 0$,

$$\begin{aligned}
\mathcal{P}(\nu_a \rightarrow \nu_b) &\approx P^{ab}|_{\xi_i = \sin^2 \theta_{13} = 0} \\
&+ \sin^2 \theta_{13} \frac{dP^{ab}}{d\xi_i}|_{\xi_i = 0} .
\end{aligned} \tag{34}$$

Because this expansion involves the *total* derivative, $dP^{ab}/d\xi$, the expanded eigenvalues are not used explicitly [7, 8].

The expression for $S'(t, t_0)$ is found from the solution of the time-dependent Schroedinger equation given in Eq. (A.9) of Ref. [7],

$$i \frac{d}{dt} S'_0(t, t_0) = H'_0 S'_0(t, t_0) , \tag{35}$$

with the Hamiltonian H'_0 , expressed in the neutrino

mass basis given in Eq. (A.6),

$$\begin{aligned}
H'_0 &= \frac{\Delta}{2} \\
&\times \begin{pmatrix} -\alpha \cos 2\theta_{12} + \hat{A} & \alpha \sin 2\theta_{12} \\ \alpha \sin 2\theta_{12} & \alpha \cos 2\theta_{12} - \hat{A} \end{pmatrix} ,
\end{aligned} \tag{36}$$

where

$$\Delta \equiv \frac{m_3^2 - m_1^2}{2E} . \tag{37}$$

The solution of Eq. (35), Eq. (22) of Ref. [7],

$$S'_0(t, t_0) = \begin{pmatrix} \alpha(t, t_0) & \beta(t, t_0) \\ -\beta^*(t, t_0) & \alpha^*(t, t_0) \end{pmatrix} , \tag{38}$$

is expressed in terms of $\alpha(t, t_0)$ and $\beta(t, t_0)$. The quantities $\alpha(t, t_0)$ and $\beta(t, t_0)$, which may be found in closed form, determine S^{ab} to leading order in $\sin \theta_{13}$,

$$S'(t, t_0) = \begin{pmatrix} \alpha & S_{12} \\ S_{21} & S_{22} \end{pmatrix} . \tag{39}$$

All higher-order corrections are contained in the transformation that rotates S'_0 back to the original flavor basis.

Defining the baseline L in terms of the time $t - t_0$ for the neutrinos to travel between their production target and detector in a uniform medium, as in Eq. (11), all quantities become functions of L . In particular, $S_{12}(t, t_0) \rightarrow S_{12}(L)$, where

$$S_{12}(L) = \cos \theta_{23} \beta(L) - i \sin \theta_{23} A(L) . \tag{40}$$

The quantity $A(L) = aA_a(L) + bA_b(L)$ is given as the first expression in Eq. (A.14) of Ref. [7], with $A_a(L)$ defined in Eq. (A.16) and $A_b(L)$ in Eq. (A.17). These quantities may be calculated analytically as integrals over L involving $f(L)$,

$$f(L) = e^{-i\bar{\Delta}L} , \tag{41}$$

$\alpha(L)$, and $\beta(L)$. We have solved these equations for $S'(t, t_0)$ exactly, and all numerical AHLO results are obtained from these expressions. These resulting expressions are, however, very complicated and too awkward to use in practice. We have used them because our only interest here is to benchmark Refs [7, 8]. Simplified expressions for the matrix element S_{12} , which describes $\nu_\mu \rightarrow \nu_e$ transitions, were used in Refs. [12–15]. Because these expressions entail a yet further set of approximations, for the purpose of this paper it serves no purpose to examine these simplified expressions.

Below, we numerically compare the oscillation probability obtained from $S'(t, t_0)$ to the exact one obtained from our Hamiltonian formulation. The comparison is made for the specific case of $e \rightarrow \mu$ transitions.

VI. ASSESSING THE ξ_i -EXPANDED $\mathcal{P}(\nu_i \rightarrow \nu_f)$

In Sect. VII, we compare the α -expanded oscillation probabilities, the $\sin^2 \theta_{13}$ -expanded oscillation probabilities, and the exact oscillation probabilities. From these results, we are able to identify the regions where both ξ_i -expanded oscillation probabilities might be improved by using our Hamiltonian formulation.

A. Regions of \hat{A}

We assess the expanded oscillation probabilities over specific regions of \hat{A} and Δ_L . For this purpose, the interval $\hat{A} > -0.8$, broken down into five sub-regions spanning the interval $\hat{A}_i < \hat{A} < \hat{A}_f$.

The first region is the solar resonance region containing the solar resonance at $\hat{A} = \alpha$. This region extends from $\hat{A}_i = 0$ to $\hat{A}_f = 0.1$. Motivated by the representation of the $\sin^2 \theta_{13}$ -expanded eigenvalues given in Appendix A 1, we split the solar resonance region into the deep solar resonance region, $0 < \hat{A} < \alpha$ and the far solar resonance region, $\alpha < \hat{A} < 0.1$.

The second region, the transition region, extends from $\hat{A}_i = 0.1$ to $\hat{A}_f = \hat{A}_2$, where $A_2 \approx 0.538$ is the value of \hat{A} at which the periods of the two most slowly varying Bessel functions, $j_0(\hat{\Delta}[1])$ and $j_0(\hat{\Delta}[3])$, are equal. The third region includes the atmospheric resonance at $\hat{A} = \hat{A}_0 \approx 1$ and extends from $\hat{A}_i = \hat{A}_2$, $\hat{A}_f = 1.2$. The asymptotic region in-

cludes all values of $\hat{A} > 1.2$. Finally, we consider the region extending from $\hat{A}_i = -0.8$ to $\hat{A}_f = +0.8$.

Within each region considered, Δ_L is chosen so that $\mathcal{P}(\nu_e \rightarrow \nu_\mu)$ displays the greatest sensitivity to approximations. This is assured by requiring that each of the three Bessel functions constituting the oscillation probability are of comparable size and interfere both constructively and destructively. For maximal interference, each of these Bessel functions $j_0(\Delta_\ell)$ should undergo at least one period of oscillation when the neutrino is detected at a distance Δ_L from the source. This is fully discussed in Ref. [9].

The maximal interference within the solar resonance region was determined to occur for $\Delta_L = 60$; the transition region for $\Delta_L = 17$; the atmospheric resonance region, for $\Delta_L = 4$; the asymptotic region for $\Delta_L = 4$. For the region extending from $\hat{A}_i = -0.8$ to $\hat{A}_f = +0.8$, $\Delta_L = 35$.

The Δ_L dependence is examined for two values of \hat{A} , one in the solar resonance region and one in the atmospheric resonance region. In all cases, the oscillation probability is examined for $\delta_{cp} = \pi/4$, with the other parameters taken from the SNM.

B. Extrapolations

The results shown in this paper may be extrapolated to a variety of values baselines, medium properties, and neutrino energies within the regions under using Eqs. (13,20),

$$\begin{aligned} L[\text{Km}] &= 5.04 \times 10^3 \frac{|\hat{A}|\Delta_L}{R\rho[\text{gm/cm}^3]} \\ E[\text{GeV}] &= 15.3 \frac{|\hat{A}|}{R\rho[\text{gm/cm}^3]}, \end{aligned} \quad (42)$$

for a medium described by ρ and R . Using Eq. (42), the oscillation probability may be extrapolated to a variety of values of neutrino energy, base lines, and medium properties once it is known for a specific set of values (Δ_L, \hat{A})

VII. COMPARISON OF THE FULL AND PATCHED $\mathcal{P}(\nu_e \rightarrow \nu_\mu)$ OF FREUND TO THE FULL $\mathcal{P}(\nu_e \rightarrow \nu_\mu)$ OF AHLO

In this section, we assess simplified expressions for $\mathcal{P}(\nu_e \rightarrow \nu_\mu)$ found in Refs [6–8]. These expressions are the only published attempts made to simplify the oscillation probability.

We compare the simplified $\mathcal{P}(\nu_e \rightarrow \nu_\mu)$ to the corresponding exact oscillation probability [9] evaluated with the exact eigenvalues to determine the relative and absolute accuracy of the approximate oscillation probabilities commonly used for the analysis and prediction of neutrino oscillation phenomena. From these results, one easily identifies which of the ξ_i -expanded oscillation probabilities best describes each region.

Freund's patched is shown as a short-dashed curve, his full result as a medium-dashed curve, the AHLO oscillation probability as a dot-dashed curve, and the oscillation probability of our Hamiltonian formulation [9] evaluated with the exact eigenvalues as a solid curve.

A. Δ_L Dependence of the ξ_i -Expanded $\mathcal{P}(\nu_e \rightarrow \nu_\mu)$

In this section, we compare the oscillation probabilities over intervals of Δ_L for several values of \hat{A} , one near the solar resonance and the other near the atmospheric resonance.

1. Near the Solar Resonance

We first look at the Δ_L -dependence of $P^{e \rightarrow \mu}(\Delta_L, \hat{A})$ in the solar resonance region for $\hat{A} = 0.0102$. Figure 1 shows that Freund's full α -expanded oscillation probability and his patched oscillation probability are both in reasonable agreement with the exact result for $\Delta_L < 20$, at which point both of Freund's oscillation probabilities begin to depart from the exact oscillation probability. They increasingly diverge from the exact result as Δ_L increases, which reflects the breakdown of the α -expansion in the solar resonance region. On the other hand, the AHLO result agrees with the exact result comparatively well over the entire interval of Δ_L shown.

2. Near the Atmospheric Resonance

We next look at the Δ_L -dependence of $P^{e \rightarrow \mu}(\Delta_L, \hat{A})$ in the atmospheric resonance region for $\hat{A} = 0.8$, a value of \hat{A} below the atmospheric resonance. Figure 2 shows that Freund's full α -expanded oscillation probability is in reasonable agreement with the exact result over the entire interval of Δ_L shown. On the other hand, Freund's

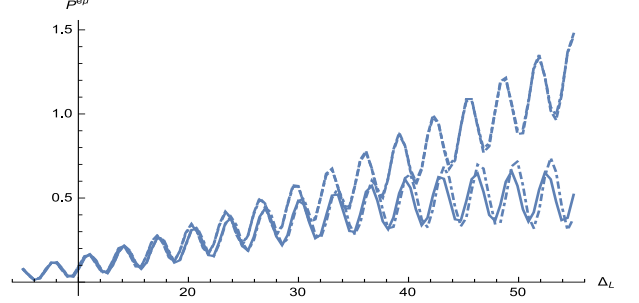


FIG. 1. $P^{e\mu}(\Delta_L, \hat{A})$ in the solar-resonance region ($\hat{A} = 0.0102$) over the interval $5 < \Delta_L < 55$ for neutrinos in matter. Parameters are taken from the SNM. Exact result (solid curve). Patched α -expanded result of Freund [6] (short-dashed curve). Full α -expanded result of Freund [6] (medium-dashed curve). Full $\sin^2 \theta_{13}$ result of AHLO [7] (dot-dashed curve)

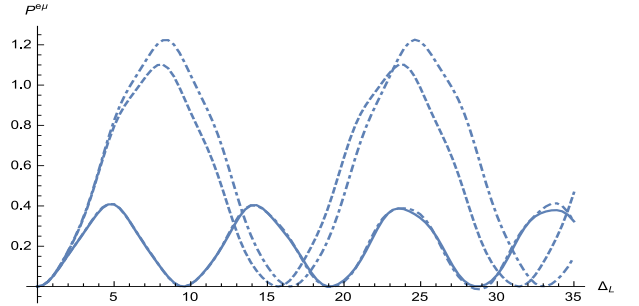


FIG. 2. Freund $P^{e\mu}(\Delta_L, \hat{A})$ in the atmospheric resonance region ($\hat{A} = 0.8$) over the interval $0 < \Delta_L < 35$ for neutrinos in matter. Parameters are taken from the SNM. Exact result (solid curve). Patched α -expanded result of Freund [6] (short-dashed curve). Full α -expanded result of Freund [6] (medium-dashed curve). Full $\sin^2 \theta_{13}$ result of AHLO [7] (dot-dashed curve)

patched α -expanded oscillation probability and the AHLO result are quite similar but are in substantial disagreement with the exact result over the same interval of Δ_L .

B. The \hat{A} Dependence of the ξ_i -Expanded $\mathcal{P}(\nu_i \rightarrow \nu_f)$

Below, we examine the \hat{A} dependence over the five regions defined earlier.

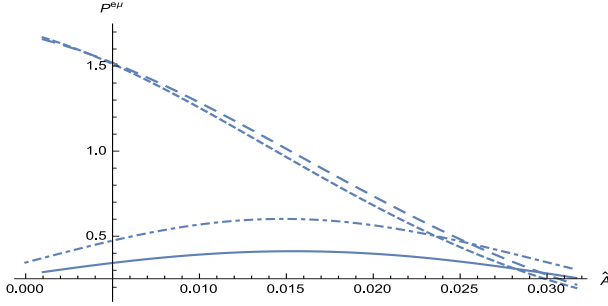


FIG. 3. $P^{e\mu}(\Delta_L, \hat{A})$ over the deep solar resonance region, $0 < \hat{A} < \alpha$, with $\Delta_L = 60$ for neutrinos in matter. Parameters are taken from the SNM. Exact result (solid curve). Patched α -expanded result of Freund [6] (short-dashed curve). Full α -expanded result of Freund [6] (medium-dashed curve). Full $\sin^2 \theta_{13}$ result of AHLO [7] (dot-dashed curve)

1. Solar Resonance Region: $0 < \hat{A} < 0.1$

The deep solar resonance region, which extends over the interval $0 < \hat{A} < \alpha$, is shown in Fig. 3. The far solar resonance region, which extends over the interval $\alpha < \hat{A} < 0.1$, is shown in Fig. 4. The results of Freund [6] and AHLO [7] are compared to the exact result within these two regions. The α -expansion is known to fail within the solar resonance region. [9] because one of the eigenvalue branch point lies at $\alpha = 0$.

Although Freund asserts that his results fails only below the solar resonance, $\hat{A} < \alpha$, it is clear from Fig. 4 that the α -expanded results are poor approximation out to $\hat{A} \approx 0.1$. The failure becomes increasingly severe as $\alpha \rightarrow 0$. This is evident for both Freund's patched and full results.

Clearly, the full $\sin^2 \theta_{13}$ -expanded result of AHLO does much better within the solar resonance region. However, Fig. 3 shows that the AHLO result does not approach the exact result in the limit $\alpha \rightarrow 0$.

2. $0.1 < \hat{A} < \hat{A}_2$

In Fig. 5, we compare the oscillation probabilities within the transition region. Comparing the short-dashed and medium-dashed curves to the solid curve, it is clear that Freund's patched and full results agree well with the exact result for $0.1 < \hat{A} < 0.3$, but for larger values of \hat{A} his patched result increasingly departs from the exact result, whereas his full result tracks the exact result throughout the

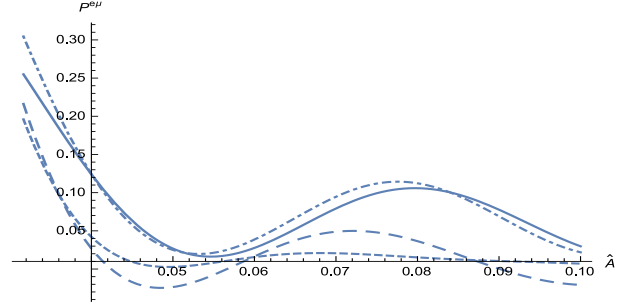


FIG. 4. $P^{e\mu}(\Delta_L, \hat{A})$ over the far solar resonance region, $\alpha < \hat{A} < 0.1$ with $\Delta_L = 60$ for neutrinos in matter. Parameters are taken from the SNM. Exact result (solid curve). Patched α -expanded result of Freund [6] (short-dashed curve). Full α -expanded result of Freund [6] (medium-dashed curve). Full $\sin^2 \theta_{13}$ result of AHLO [7] (dot-dashed curve)

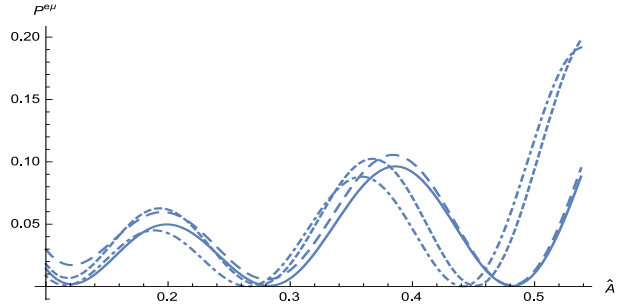


FIG. 5. $P^{e\mu}(\Delta_L, \hat{A})$ for $\Delta_L = 17$ over the transition region, $0.1 < \hat{A} < \hat{A}_2$, for neutrinos in matter. Parameters are taken from the SNM. Exact result (solid curve). Patched α -expanded result of Freund [6] (short-dashed curve). Full α -expanded result of Freund [6] (medium-dashed curve). Full $\sin^2 \theta_{13}$ result of AHLO [7] (dot-dashed curve)

transition region.

Comparing the dot-dashed and solid curves, it is clear that that Freund's patched and the AHLO result provide rather similar descriptions of the oscillation probability throughout the transition region.

3. $\hat{A}_2 < \hat{A} < 1.2$

In Fig. 6, we compare the oscillation probabilities over the atmospheric resonance region. Comparing the dot-dashed and medium-dashed curves, it is clear that that the departure of Freund's full result from his patched result continues to increase across the atmospheric resonance region. Compar-

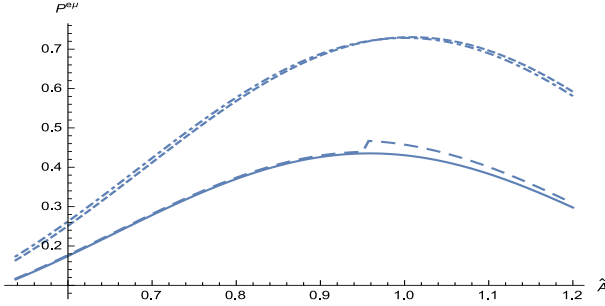


FIG. 6. $P^{e\mu}(\Delta_L, \hat{A})$ for $\Delta_L = 4$ over the atmospheric resonance region, $\hat{A}_2 < \hat{A} < 1.2$, for neutrinos in matter. Parameters are taken from the SNM. Exact result (solid curve). Patched α -expanded result of Freund [6] (short-dashed curve). Full α -expanded result of Freund [6] (medium-dashed curve). Full $\sin^2 \theta_{13}$ result of AHLO [7] (dot-dashed curve)

ing the dot-dashed and solid curves, it is clear that that Freund's patched and the AHOL result continue to provide rather similar descriptions of the oscillation probability throughout the atmospheric resonance region.

Freund's full result provides a reasonable description of the exact result below the atmospheric resonance, at which point his result is discontinuous and lies above the exact result for larger values of \hat{A} .

4. $1.2 < \hat{A} < 2.5$

In Fig. 7, we compare the oscillation probabilities over a portion of the asymptotic region. Comparing the dot-dashed and short-dashed curves, we see once again the departure of Freund's patched result from his patched result. However, this departure appears to decrease above the atmospheric resonance region and approaches the exact result for the larger values of \hat{A} .

5. $-0.8 < \hat{A} < 0.8$

Because the branch point of the α expansion occurs for $\hat{A} = 0$, it will adversely impact the total oscillation probability for both neutrinos and anti-neutrinos. This is confirmed in Fig. 8.

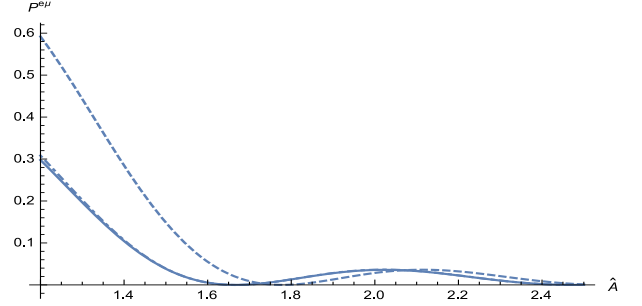


FIG. 7. $P^{e\mu}(\Delta_L, \hat{A})$ vs \hat{A} for $\Delta_L = 4$ within the asymptotic region, $1.2 < \hat{A} < 2.5$ for neutrinos in matter. Parameters are taken from the SNM. Exact result (solid curve). Patched α -expanded result of Freund [6] (short-dashed curve). Full α -expanded result of Freund [6] (medium-dashed curve). Full $\sin^2 \theta_{13}$ result of AHLO [7] (dot-dashed curve)

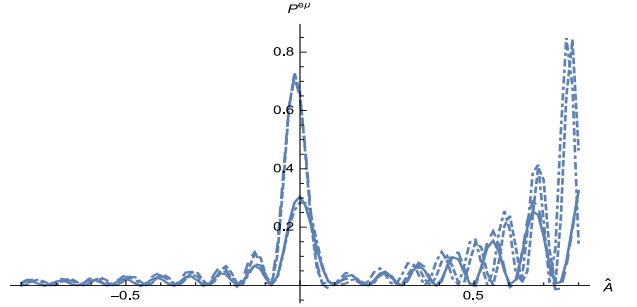


FIG. 8. $P^{e\mu}(\Delta_L, \hat{A})$ over the interval $-0.8 < \hat{A} < 0.8$ with $\Delta_L = 35$ for neutrinos in matter. Parameters are taken from the SNM. Exact result (solid curve). Patched α -expanded result of Freund [6] (short-dashed curve). Full α -expanded result of Freund [6] (medium-dashed curve). Full $\sin^2 \theta_{13}$ result of AHLO [7] (dot-dashed curve)

C. Discussion

In this section, we calibrated the accuracy of Freund's [6] full and patched exact oscillation probabilities and the full AHLO [7] oscillation probability. We were able to identify which of the approximate solutions best described the exact result within and above the solar resonance region. Few studies of this nature have ever been made.

Freund's patched result was found to be significantly less accurate than the full result in all regions. Freund's full result was calculated and compared to the exact result in all regions, including the solar resonance region. The failure of Freund's full result within the solar resonance region is evident

from Figs. 3,4; we also confirmed that the $\sin^2 \theta_{13}$ expansion leads to inaccuracy in the vicinity of the atmospheric resonance. Both inaccuracies grow as \hat{A} approaches the branch points.

In the vicinity of the atmospheric resonance, $\hat{A} \approx \cos 2\theta_{13}$, we found that neither the AHLO result nor the full result of Freund provides a very good description of the oscillation probability. This is expected for the $\sin^2 \theta_{13}$ expansion because the corresponding branch point lies close to the atmospheric resonance. Freund's full result is discontinuous at the position of the atmospheric resonance. This discontinuity is quite noticeable when the Daya Bay value of θ_{13} is adopted.

It was clear from our calculations that our Hamiltonian formulation needs no patch to avoid any discontinuity such as that present in Freund's full result.

Freund, in his paper [6], does actually compare his full and patched results to an exact calculation of the oscillation probability [his Fig. (1)]. His results, when viewed casually, may appear inconsistent with those given here, especially with regard to the theoretical error of his patched result.

However, one should note that Freund's comparisons are presented on a logarithmic plot of multiple decades, whereas ours are given on a linear plot. On a logarithmic scale, factors of two are often get lost in the noise. Additionally, Freund considers a broad range of model parameters, which makes it difficult to pinpoint the portion of his presentation that reflects the SNM, which is of course the model underlying our analysis.

We also found that the $\sin^2 \theta_{13}$ expansion [7, 8] represents of the exact oscillation probability relatively accurately within the solar resonance region, but its accuracy in other regions is comparable to Freund's patched result. We also found that in the region between the solar and atmospheric resonances, $0.1 < \hat{A} < \hat{A}_2$, the expansion in α is a good representation of the exact result, whereas the expansion in $\sin^2 \theta_{13}$ rapidly deteriorates with increasing \hat{A} .

In the vicinity of the atmospheric resonance, $\hat{A} \approx \cos 2\theta_{13}$, we found that neither the AHLO result nor the full Freund result provides a very good description of the oscillation probability. This is expected for the $\sin^2 \theta_{13}$ expansion because the corresponding branch point lies close to the atmospheric resonance. A careful reading of Ref. [6] reveals that some inaccuracy of the α expansion would have been anticipated there in light of the Daya Bay result [19], but its extent may be a surprising disappointment

to some. The *asymptotic* region, $\hat{A} > 2.0$ is shown in Fig. 7.

Even though expanded eigenvalues are not used explicitly for the $\sin^2 \theta_{13}$ -expanded oscillation probability, Eq. (34) is still a poor representation of the exact result in the vicinity of the branch point at $\hat{A} = \hat{A}_0$, where the eigenvalue expansion fails. To separate the theoretical errors into those arising from the expansion of the oscillation probability from those arising from the expansion of the eigenvalues we have relied on the numerical techniques.

VIII. APPROXIMATE FORMULATION OF $\mathcal{P}(\nu_i \rightarrow \nu_f)$ ACCURATE TO A FEW PERCENT

Because subtle but important trends are more easily identified by examining analytic expressions than by scanning through numerical lists, simpler and most accurate analytic expressions would be significant considering that higher quality data are expected to become available at future neutrino facilities. In our original publication [9], we compare exact oscillation probabilities to those found from our Hamiltonian formulation evaluated with ξ -expanded eigenvalues.

A. Above the Solar Resonance Region, $\hat{A} > 0.1$

In our original publication [9], we find that the errors of $O(\alpha^2)$ expected in regions sufficiently remote from the branch point of the α -expanded eigenvalues obtain for $\hat{A} > 0.1$. From this we estimate that simple analytic expressions for the oscillation probability accurate to a few percent are quite likely over this region using our Hamiltonian formulation [9].

To identify the regions where expressions for the oscillation probability of our Hamiltonian formulation [9] are improvements over simplified oscillation probabilities found by Freund. [6], we need to examine the accuracy of Freund's full and patched oscillation probabilities. Figures presented in Sect. VII assess this accuracy. Because the accuracy of Freund's patched oscillation probabilities is found to be vastly inferior to that of his full oscillation probability, his patched oscillation probabilities are not further considered.

The full α -expanded oscillation probability of Freund [6] is compared to the exact oscillation probability over the interval $0.1 < \hat{A} < \hat{A}_2$ in Fig. 5 of the present paper. We see from this figure that Freund's full oscillation probability [6] becomes increasingly

less accurate as $\hat{A} \rightarrow 0.1$. On the other hand, the oscillation probability of our Hamiltonian formulation evaluated with α -expanded eigenvalues, which is compared to the exact oscillation probability over the same interval in Fig. 4 of Ref. [9], remains quite accurate as $\hat{A} \rightarrow 0.1$. We conclude from these results that simple expressions for the oscillation probability more accurate than Freund's full result over this interval may be found using the results our Hamiltonian formulation.

Freund's full oscillation probability [6] is compared to the exact oscillation probability in the vicinity of the atmospheric resonance in Fig. 6 of the present paper. We see there that Freund's full oscillation probability [6] is discontinuous at the location of the atmospheric resonance, whereas the oscillation probability obtained from our Hamiltonian formulation evaluated with α -expanded eigenvalues given in Fig. 6 of our original paper [9] is continuous throughout the atmospheric resonance region. Because it is also a very accurate representation of the exact result, we conclude that simple expressions for the oscillation probability that are more accurate than Freund's full result in the vicinity of the atmospheric resonance may be found using the results our Hamiltonian formulation.

The full α -expanded oscillation probability of Freund [6] is compared to the exact oscillation probability for asymptotic values of \hat{A} in Fig. 7 of the present paper. We see from this figure and Fig. 7 of our original paper [9] that Freund's full oscillation probability [6] and that obtained from our Hamiltonian formulation evaluated with α -expanded eigenvalues are of comparable accuracy for asymptotic values of \hat{A} . We conclude that simple expressions for the oscillation probability of accuracy comparable to Freund's full result may be found using the results our Hamiltonian formulation for asymptotic values of \hat{A} .

In our original publication [9], we also compare exact oscillation probabilities to those found from our Hamiltonian formulation evaluated with $\sin^2 \theta_{13}$ -expanded eigenvalues. The accuracy with which the oscillation probability of our Hamiltonian formulation evaluated with $\sin^2 \theta_{13}$ -expanded eigenvalues reproduces the exact oscillation probability is strikingly good over the region $0.1 < \hat{A} < \hat{A}_2$, as seen in Fig. 4 of our original paper. This establishes that simple and accurate analytic expressions for the oscillation probability are also likely to be found somewhat above the solar resonance region using results of our Hamiltonian formulation [9] with $\sin^2 \theta_{13}$ -expanded eigenvalues.

B. Solar Resonance Region, $0 < \hat{A} < 0.1$

Similar considerations apply to $\sin^2 \theta_{13}$ -expanded oscillation probabilities. Close agreement between the exact oscillation probability and those of our Hamiltonian formulation evaluated with $\sin^2 \theta_{13}$ -expanded eigenvalues is seen over the region $0 < \hat{A} < 0.1$ seen in Fig. 3 of our original paper [9]. This suggests that simpler and most accurate analytic expressions for the oscillation probability within the solar resonance region are likely to be found using results obtained from our Hamiltonian formulation [9].

The figures in our original paper [9] also show that for values of \hat{A} closer to the branch point of the $\sin^2 \theta_{13}$ -expanded eigenvalues, the accuracy of the oscillation probabilities deteriorate rather rapidly.

As before, to identify the regions where expressions for the oscillation probability obtained from our Hamiltonian formulation [9] are improvements over simplified oscillation probabilities found by AHLO [7], we need to examine the accuracy of the full AHLO oscillation probabilities. Figures presented in Sect. VII assess this accuracy.

We see from the results appearing in Figs. 3 to Fig. 7 of the present paper that the full $\sin^2 \theta_{13}$ -expanded oscillation probability of AHLO agrees rather poorly with the exact result over all regions except for the far solar resonance region. Within the far solar resonance region, the full $\sin^2 \theta_{13}$ -expanded oscillation probability of our Hamiltonian formulation [7] is reasonably accurate.

From these results, we conclude that simple expressions of accuracy greater than a few percent are likely to be found from the results our Hamiltonian formulation evaluated with $\sin^2 \theta_{13}$ -expanded eigenvalues. Such oscillation probabilities would then be vastly more accurate than those of AHLO [7].

IX. SUMMARY AND CONCLUSIONS

In this paper, we assessed the theoretical errors of simplified neutrino oscillation probabilities obtained from various approximate formulations. The errors of the simplified oscillation probabilities obtained in Refs. [6–8] are associated, in large part, with branch points [9] of the medium-modified neutrino eigenvalues. Currently, there is essentially no understanding of the errors of these simplified oscillation probabilities. We also assessed the likelihood that simple analytical approximations to three-flavor neutrino oscillation probabilities with accuracy of a few percent would be found using our recent Hamiltonian formu-

lation [9]. We considered flavor-changing transitions in the (ν_e, ν_μ) sector within the Standard Neutrino Model, the only cases considered in Refs. [6–8].

We compared the approximate results over various regions of \hat{A} to identify which gave the best description of the exact results. From this comparison, we found that the full results of Freund are satisfactory everywhere except for the solar- and atmospheric-resonance regions. Those of AHLO describe the solar-resonance region well, but they are complicated and rapidly deteriorate outside this region. The simple neutrino oscillation probabilities of the approximate formulation we propose in Sect. VIII are accurate to a few percent errors within essentially all regions of interest.

We thus conclude from Sect. VIII that our Hamiltonian formulation offers the opportunity to obtain approximate oscillation probabilities vastly more accurate than those presently available. This result is significant because it would obviate the need for exact computer simulations under many circumstances, thus simplifying analysis and prediction at current and future and next-generation neutrino neutrino facilities.

Making use of the guidance provided by the results of this paper, in future work [16] we derive simple approximations with few percent errors within essentially all regions of interest using our Hamiltonian formulation.

Appendix A: Oscillation Probability in Our Hamiltonian Formulation

In this appendix, we give alternative expressions for the $\sin^2 \theta_{13}$ -expanded eigenvalues equivalent to those given in Ref. [9]. Separate expressions are given for \hat{A} above and below $\hat{A} = \alpha$ in terms of the ratio of the small parameters of the SNM, $R_p \equiv \sin^2 \theta_{13}/\alpha \approx 0.7$

1. Alternative Representation for the $\sin^2 \theta_{13}$ -Expanded Eigenvalues

We introduce the notation $\hat{E}_{\theta\ell}^L$ to represent the $\sin^2 \theta_{13}$ -expanded eigenvalues \hat{E}_ℓ for $\hat{A} < \alpha$, and $\hat{E}_{\theta\ell}^G$ to represent them for $\hat{A} > \alpha$. The representation of \hat{E}_ℓ given in terms of $\hat{E}_{\theta\ell}^L$ and $\hat{E}_{\theta\ell}^G$ is equivalent to the representation \hat{E}_ℓ given in Ref. [9].

$$a. \quad \hat{A} < \alpha$$

The following expressions for $\hat{E}_{\theta\ell}^L$ are found by replacing $\hat{A} \rightarrow \alpha R_s$ and $\hat{C}_\theta \rightarrow \alpha C_T$ in \hat{E}_ℓ given in Ref. [9],

$$\begin{aligned} \hat{E}_{\theta 1}^L &= \frac{\alpha}{2}(R_s + 1 - C_T) \\ &\quad + \frac{\alpha R_p R_s}{2(1-y)C_T}(2 - \hat{A}_0 - \alpha - \alpha C_T) \\ &\quad + \frac{R_p y}{2C_T}(2 - 4\hat{A}_0 + \hat{A}_0^2 - 2\alpha + 2\hat{A}_0\alpha) \\ \hat{E}_{\theta 2}^L &= \frac{\alpha}{2}(R_s + 1 + C_T) \\ &\quad - \frac{\alpha R_p R_s}{2(1-y)C_T}(2 - \hat{A}_0 - \alpha + \alpha C_T) \\ &\quad - \frac{R_p y}{2C_T}(2 - 4\hat{A}_0 + \hat{A}_0^2 - 2\alpha + 2\hat{A}_0\alpha) \\ \hat{E}_{\theta 3}^L &= 1 + \frac{\alpha^2 R_p R_s}{1-y}. \end{aligned} \quad (A1)$$

$$b. \quad \hat{A} > \alpha$$

The following expressions for $\hat{E}_{\theta\ell}^G$ are found by replacing $\hat{A} \rightarrow \alpha/R_s$ and $\hat{C}_\theta \rightarrow \hat{A}C_T$ in \hat{E}_ℓ given in Ref. [9],

$$\begin{aligned} \hat{E}_{\theta 1}^G &= \frac{\alpha}{2R_s}(R_s + 1 - C_T) \\ &\quad + \frac{\alpha R_p}{2R_s(1-y)C_T}(2R_s - \hat{A}_0 R_s - \alpha R_s - \alpha C_T) \\ &\quad + \frac{y R_s R_p}{2C_T}(2 - 4\hat{A}_0 + \hat{A}_0^2 - 2\alpha + 2\hat{A}_0\alpha) \\ \hat{E}_{\theta 2}^G &= \frac{\alpha}{2R_s}(R_s + 1 + C_T) \\ &\quad - \frac{\alpha R_p}{2R_s(1-y)C_T}(2R_s - \hat{A}_0 R_s - \alpha R_s + \alpha C_T) \\ &\quad - \frac{y R_s R_p}{2C_T}(2 - 4\hat{A}_0 + \hat{A}_0^2 - 2\alpha + 2\hat{A}_0\alpha) \\ \hat{E}_{\theta 3}^G &= 1 + \frac{\alpha^2 R_p}{R_s(1-y)}. \end{aligned} \quad (A2)$$

c. Discussion

Because Eqs. (A1,A2) are equivalent representations of the eigenvalues \hat{E}_ℓ and their differences, they

are accurate to a few percent for $\hat{A} < 0.6$. The following points are also worthy of noting.

The same quantity

$$C_T \equiv \sqrt{1 + R_s^2 - 2R_s \cos \theta_{12}} \approx 1, \quad (\text{A3})$$

appears in the expressions for the eigenvalues for both $\hat{A} < \alpha$ and $\hat{A} > \alpha$.

Above the branch point at $y = 1$, $\hat{E}_{\theta\ell}^L$ and $\hat{E}_{\theta\ell}^G$ are related:

- (1) $\hat{E}_{\theta 2} = \hat{E}_{\theta 1}|_{C_T \rightarrow -C_T}$ and
- (2) $\hat{E}_{\theta 3}$ and $\hat{E}_{\theta 2}$ exchange roles.

Appendix B: Exact Analytic Results for the Coefficients $w_i^{(mn)}[\ell]$

Full expressions for the coefficients $w_{i;n}^{(mn)}$ appearing in the expressions for the partial oscillation probabilities of Ref. [9] are given in this appendix. They are expressed in terms parameters of the SNM and the following functions of them,

$$\begin{aligned} C_1^{(\pm)} &\equiv \cos^2 \theta_{12} \cos^2 \theta_{23} \pm \sin^2 \theta_{23} \sin^2 \theta_{12} \sin^2 \theta_{13} \\ C_2^{(\pm)} &\equiv \cos^2 \theta_{12} \pm \sin^2 \theta_{12} \sin^2 \theta_{13}, \end{aligned} \quad (\text{B1})$$

where $C_2^{(\pm)}$ was defined earlier in Eq. (??). In the SNM, many of the terms in $w_{i;n}^{(mn)}$ are quite small and may be dropped in practice.

1. Coefficients $w_{\cos^2}^{(mn)}$

$$\begin{aligned} w_{\cos^2;0}^{(22)} &= \frac{\hat{A}\alpha^2}{4} \cos^2 \theta_{13} \sin^2 2\theta_{12} \sin^2 \theta_{13} (1 - \alpha \sin^2 \theta_{12}) \\ w_{\cos^2;1}^{(22)} &= -\frac{\alpha^3}{4} \sin^2 2\theta_{12} \sin^2 \theta_{13} \\ w_{\cos^2;2}^{(22)} &= \frac{\alpha^2}{4} \sin^2 2\theta_{12} \sin^2 \theta_{13} \end{aligned} \quad (\text{B2})$$

2. Coefficients $w_{\cos}^{(mn)}$

$$\begin{aligned} w_{\cos;0}^{(12)} &= -\frac{\alpha}{8} \cos \theta_{13} \sin 2\theta_{12} \sin 2\theta_{13} ((1 - \alpha)^2 - \hat{A}(\cos 2\theta_{13} + \alpha(1 - 2 \cos 2\theta_{13} \sin^2 \theta_{12}) \\ &\quad - 2\alpha^2 \sin^2 \theta_{12} C_2^{(+)})) \\ w_{\cos;1}^{(12)} &= -\frac{\alpha}{8} \cos \theta_{13} \sin 2\theta_{12} \sin 2\theta_{13} (1 + \alpha - 2\alpha^2 \sin^2 \theta_{12}) - \hat{A}w_{\cos;2}^{(12)} \\ w_{\cos;2}^{(12)} &= \frac{\alpha}{4} \cos \theta_{13} \sin 2\theta_{12} \sin 2\theta_{13} (1 - \alpha \sin^2 \theta_{12}), \end{aligned} \quad (\text{B3})$$

$$\begin{aligned} w_{\cos;0}^{(23)} &= \frac{\alpha}{8} \cos \theta_{13} \cos 2\theta_{23} \sin 2\theta_{12} \sin 2\theta_{13} ((1 - \alpha)^2 - \hat{A}(\cos 2\theta_{13} - \alpha(1 - 4 \sin^2 \theta_{12} \sin^2 \theta_{13}) \\ &\quad + 2\alpha^2 \sin^2 \theta_{12} C_2^{(-)})) \\ w_{\cos;1}^{(23)} &= \frac{\alpha}{4} \cos 2\theta_{23} \sin 2\theta_{12} \sin \theta_{13} (\cos^2 \theta_{13} + \alpha \cos^2 \theta_{13} - 2\alpha^2 C_2^{(-)}) \\ w_{\cos;2}^{(23)} &= -\frac{\alpha}{2} \cos 2\theta_{23} \sin 2\theta_{12} \sin \theta_{13} (\cos^2 \theta_{13} - \alpha C_2^{(-)}), \end{aligned} \quad (\text{B4})$$

$$\begin{aligned}
w_{cos;0}^{(22)} &= \frac{\alpha}{2} \sin \theta_{13} \sin 2\theta_{12} \cos^2 \theta_{13} ((1-\alpha)^2 \sin^2 \theta_{23} - \hat{A}(\cos 2\theta_{13} \sin^2 \theta_{23} \\
&\quad + \alpha(\cos^2 \theta_{12} - \sin^2 \theta_{23}(1 - 4\sin^2 \theta_{12} \sin^2 \theta_{23})) - 2\alpha^2 \sin^2 \theta_{12} C_1^{(+)}) \\
w_{cos;1}^{(22)} &= \frac{\alpha}{2} \sin 2\theta_{12} \sin \theta_{13} (\sin^2 \theta_{23} \cos^2 \theta_{13} + \alpha \cos^2 \theta_{13} \sin^2 \theta_{23} - \alpha^2(1 - 2C_1^{(+)}) \\
&\quad + \hat{A} \cos^2 \theta_{13} (1 - \alpha \sin^2 \theta_{12})) \\
w_{cos;2}^{(22)} &= -\frac{\alpha}{2} \sin 2\theta_{12} \sin \theta_{13} (2 \cos^2 \theta_{13} \sin^2 \theta_{23} - \alpha(1 - 2C_1^{(+)}) .
\end{aligned} \tag{B5}$$

The coefficients $w_{cos}^{(33)}$ are obtained from $w_{cos}^{(22)}$ by making the replacement $\sin \theta_{23} \leftrightarrow \cos \theta_{23}$ and by flipping the overall sign.

3. Coefficients $w_0^{(mn)}$

$$\begin{aligned}
w_{0;0}^{(12)} &= \frac{\alpha}{4} (1-\alpha)^2 \sin^2 \theta_{12} \sin^2 2\theta_{13} \sin^2 \theta_{23} + \frac{1}{4} \hat{A} \cos^2 \theta_{13} (\sin^2 2\theta_{13} \sin^2 \theta_{23} - 4\alpha \sin^2 \theta_{12} \sin^2 \theta_{13} \sin^2 \theta_{23} \\
&\quad \times (2 - 3\sin^2 \theta_{13}) - 4\alpha^2 \sin^2 \theta_{12} \sin^2 \theta_{13} (C_1^{(+)} + \sin^2 \theta_{23} \cos 2\theta_{12} - \sin^2 \theta_{23} C_2^{(-)} + \sin^2 \theta_{23} C_2^{(+)}) \\
&\quad + 4\alpha^3 \sin^2 \theta_{12} C_1^{(+)} C_2^{(+)}) \\
w_{0;1}^{(12)} &= -\cos^2 \theta_{13} (\sin^2 \theta_{13} \sin^2 \theta_{23} - \alpha \sin^2 \theta_{12} \sin^2 \theta_{13} \sin^2 \theta_{23} - \alpha^2 \sin^2 \theta_{12} \sin^2 \theta_{13} \sin^2 \theta_{23} \\
&\quad + \alpha^3 \sin^2 \theta_{12} C_1^{(+)}) - \hat{A} w_{0;2}^{(12)} \\
w_{0;2}^{(12)} &= \cos^2 \theta_{13} (\sin^2 \theta_{13} \sin^2 \theta_{23} - 2\alpha \sin^2 \theta_{12} \sin^2 \theta_{13} \sin^2 \theta_{23} + \alpha^2 \sin^2 \theta_{12} C_1^{(+)}) ,
\end{aligned} \tag{B6}$$

The coefficients $w_0^{(13)}$ are obtained from $w_0^{(12)}$ by making the replacement $\sin \theta_{23} \leftrightarrow \cos \theta_{23}$.

$$\begin{aligned}
w_{0;0}^{(23)} &= \frac{\alpha}{4} (1-\alpha)^2 \sin^2 2\theta_{23} \cos^2 \theta_{13} C_2^{(-)} \\
&\quad - \frac{1}{4} \hat{A} \cos^2 \theta_{13} (\cos^2 \theta_{13} \sin^2 2\theta_{23} \sin^2 \theta_{13} - \alpha \sin^2 \theta_{13} \sin^2 2\theta_{23} (1 + \sin^2 \theta_{12} - 3\sin^2 \theta_{12} \sin^2 \theta_{13}) \\
&\quad - \alpha^2 (\sin^2 2\theta_{12} \sin^2 \theta_{13} + \sin^2 \theta_{12} \sin^2 2\theta_{23} (1 - 3\sin^2 \theta_{13}) C_2^{(-)}) \\
&\quad + \alpha^3 \sin^2 \theta_{12} (\sin^2 2\theta_{12} \sin^2 \theta_{13} + \sin^2 2\theta_{23} + C_2^{(-)2})) \\
w_{0;1}^{(23)} &= -\frac{1}{4} (\cos^4 \theta_{13} \sin^2 2\theta_{23} - \alpha \cos^2 \theta_{13} \sin^2 2\theta_{23} C_2^{(-)} \\
&\quad - \alpha^2 \cos^2 \theta_{13} \sin^2 2\theta_{23} C_2^{(-)} + \alpha^3 (\sin^2 2\theta_{12} \sin^2 \theta_{13} + \sin^2 2\theta_{23} C_2^{(-)2})) \\
w_{0;2}^{(23)} &= \frac{1}{4} (\cos^4 \theta_{13} \sin^2 2\theta_{23} - 2\alpha C_2^{(-)} \cos^2 \theta_{13} \sin^2 2\theta_{23} + \alpha^2 (\sin^2 2\theta_{12} \sin^2 \theta_{13} \\
&\quad + \sin^2 2\theta_{23} C_2^{(-)2})) ,
\end{aligned} \tag{B7}$$

$$\begin{aligned}
w_{0;0}^{(11)} &= -\frac{\alpha}{4} (1-\alpha)^2 \sin^2 \theta_{12} \sin^2 2\theta_{13} - \frac{1}{4} \hat{A} \cos^2 \theta_{13} (\sin^2 2\theta_{13} - 2\alpha \sin^2 \theta_{12} \sin^2 \theta_{13} (1 + 3\cos 2\theta_{13}) \\
&\quad - 4\alpha^2 \sin^2 \theta_{12} \sin^2 \theta_{13} (1 + \cos^2 \theta_{12} - \sin^2 \theta_{12} (2 - 3\sin^2 \theta_{13})) + 4\alpha^3 \sin^2 \theta_{12} C_2^{(+2)}) \\
w_{0;1}^{(11)} &= \cos^2 \theta_{13} (\sin^2 \theta_{13} - \alpha \sin^2 \theta_{12} \sin^2 \theta_{13} - \alpha^2 \sin^2 \theta_{12} \sin^2 \theta_{13} + \alpha^3 \sin^2 \theta_{12} C_2^{(+)}) \\
&\quad - \hat{A} w_{0;2}^{(11)} \\
w_{0;2}^{(11)} &= -\cos^2 \theta_{13} (\sin^2 \theta_{13} - 2\alpha \sin^2 \theta_{12} \sin^2 \theta_{13} + \alpha^2 \sin^2 \theta_{12} C_2^{(+)})
\end{aligned} \tag{B8}$$

$$\begin{aligned}
w_{0;0}^{(22)} &= -\alpha(1-\alpha)^2 \cos^2 \theta_{13} \sin^2 \theta_{23} C_1^{(+)} - \hat{A} \cos^2 \theta_{13} (\cos^2 \theta_{13} \sin^2 \theta_{13} \sin^4 \theta_{23} \\
&\quad - \alpha \sin^2 \theta_{13} \sin^2 \theta_{23} (1 - 3C_1^{(+)} + \cos 2\theta_{12} \cos 2\theta_{23}) \\
&\quad + \alpha^2 \sin^2 \theta_{12} \sin^2 \theta_{23} (1 - 3\sin^2 \theta_{13}) C_1^{(+)} + \alpha^3 \sin^2 \theta_{12} C_1^{(+2)} \\
w_{0;1}^{(22)} &= \cos^2 \theta_{13} \cos^2 \theta_{23} (1 - \cos^2 \theta_{13} \sin^2 \theta_{23}) - \alpha \cos^2 \theta_{13} \sin^2 \theta_{23} C_1^{(+)} - \alpha^2 \cos^2 \theta_{13} \sin^2 \theta_{23} C_1^{(+)} + \alpha^3 C_1^{(+)} \\
&\quad \times (1 - C_1^{(+)}) + \hat{A} \cos^2 \theta_{13} (\sin^2 \theta_{13} \sin^2 \theta_{23} - 2\alpha \sin^2 \theta_{12} \sin^2 \theta_{13} \sin^2 \theta_{23} + \alpha^2 \sin^2 \theta_{12} C_1^{(+)}) \\
w_{0;2}^{(22)} &= -\cos^2 \theta_{13} \sin^2 \theta_{23} (1 - \cos^2 \theta_{13} \sin^2 \theta_{23}) + 2\alpha \sin^2 \theta_{23} (\cos^2 \theta_{12} \cos^2 \theta_{23} - \sin^2 \theta_{23} \sin^2 \theta_{12} \sin^4 \theta_{13} \\
&\quad - \sin^2 \theta_{13} (\cos^2 \theta_{12} - \sin^2 \theta_{23})) - \alpha^2 C_1^{(+)} (1 - C_1^{(+)})
\end{aligned} \tag{B9}$$

The coefficients $w_0^{(33)}$ are obtained from $w_0^{(22)}$ by making the replacement $\sin \theta_{23} \leftrightarrow \cos \theta_{23}$.

-
- [1] L. Wolfenstein, Phys. Rev. **D17**, 2369 (1978).
 - [2] S. P. Mikheev and A. Yu. Smirnov, Soviet Journal Nuclear Physics 42, 913-917 (1985).
 - [3] R. Davis Jr., Phys. Rev. Lett. 12, 303-305 (1964).
 - [4] B.T. Cleveland et al., Astrophys. J. 496, 505-526 (1998).
 - [5] Irina Mocioiu and Robert Shrock, Phys. Rev. **D62**, 053017 (2000).
 - [6] M. Freund, Phys. Rev. **D64**, 053003 (2001).
 - [7] E. Akhmedov, P. Huber, M. Lindner, and T. Ohlsson, Nucl. Phys. **B608**, 394 (2001).
 - [8] M. Jacobson and T. Ohlsson, Phys. Rev. **D69**, 013003 (2004).
 - [9] M. B. Johnson, E. M. Henley, and L. S. Kisslinger, Phys. Rev. **D91**, 076005 (2015).
 - [10] The ISS Working group, arXiv:0710.4947/hep-ph.
 - [11] V. Barger, K. Whisnant, S. Pakvasa, and R. J. N. Phillips, Phys. Rev. **D22**, 2718 (1980).
 - [12] E. M. Henley, M. B. Johnson, and L. S. Kisslinger, Int J. Mod Phys. E **20**, 2463 (2011); arXiv:1102.5106/hep-ph (2011).
 - [13] L. S. Kisslinger, E. M. Henley, and M. B. Johnson, arXiv:1105.2741/hep-ph (2011).
 - [14] L. S. Kisslinger, E. M. Henley, and M. B. Johnson, Int J. Mod Phys. E **21**, 12920 (2012) (erratum); arXiv:1205.6430/hep-ph (2011).
 - [15] L. S. Kisslinger, E. M. Henley, and M. B. Johnson, Int J. Mod Phys. E **21**, 1250065 (2012); arXiv:1203.6613/hep-ph (2012).
 - [16] M. B. Johnson and L.S. Kisslinger, "Simplified Theory of Neutrino Oscillations in Matter with CP Violation," Submitted to Phys. Rev. D.
 - [17] H. Davoudiasl, H. S. Lee, and W. J. Marciano, Phys. Rev. **D84**, 013009, (2011).
 - [18] M. C. Gonzalez-Garcia, M. Maltoni, and J. Salvado, arXiv:1103.4365/hep-ph; JHEP 1105: 075 (2011).
 - [19] F.P. An et.al., Daya Bay Collaboration, Chin. Phys. C **37**, 01101 (2013); arXiv:1210.6327/hep-ex.
 - [20] A. Cervera, *et al*, Nucl. Phys. **B579**, 17 (2000).